Scaling properties and anomalous transport of particles inside the stochastic layer

G. M. Zaslavsky[1,2] and S. S. Abdullaev[1]
[1]*Courant Institute of Mathematical Sciences, New York University, New York, New York 10012*
[2]*Physics Department, New York University, New York, New York 10003*
(Received 13 September 1994; revised manuscript received 16 January 1995)

Particle motion in a two-wave field is considered as a model for studying the kinetic (transport) properties inside the stochastic layer. The existence of an exact renormalization invariance of the separatrix with respect to the perturbation parameter and the approximate renormalization invariance for the exact equation of motion near a saddle point is shown. High accuracy symplectic integration is used to obtain the distribution function, its moments, and transport exponents. Scaling properties and anomalous transport have been found. It is shown that, depending on the parameters of the system, there is a possibility of modifying the fine (islands) structure of the stochastic layer, which leads to variations of the transport properties from the anomalous to the normal (Gaussian) ones.

PACS number(s): 05.45.+b, 47.52.+j, 47.53.+n

I. INTRODUCTION

The separatrix of a Hamiltonian system splits if a periodic perturbation of a generic type influences the system [1]. It was shown in different ways that such a phenomenon leads to a replacement of the separatrix of the unperturbed system by a stochastic (ergodic) layer in the perturbed one. The layer forms a narrow band with a complicated fine structure in the phase space of the system [2–10]. It may be worth mentioning that numerous applications of the phenomenon of stochastic layer occurrence draw special attention to its properties (for a review see [11]). Among them is the problem of particle kinetics inside the stochastic layer, which has attracted researchers from the very beginning [2,12–14]. The main difficulty in the investigation of the transport (kinetic) properties of particles inside the stochastic layer can be formulated in an informal way: generally speaking, the chaotic motion component of phase space is strongly nonuniform with fractal (or maybe multifractal) alternating of fine stochastic sublayers with Kol'mogorov-Arnol'd-Moser stability islands. The motion of entangled particles between the islands constitutes the basis of the particle transport inside the stochastic layer.

An important area of application of the stochastic layer comes from the fusion program, where the so-called ergodic divertor is created and studied in different tokamaks to resolve the problem of high energy deposition from particles at the plasma edge [15]. One remembers the beginning of the tokamak and stellarator eras when the problem of magnetic separatrix destruction initiated the research of chaos and homoclinics. A more recent interest in the problem is strongly related to deeper and finer properties of long time asymptotics of particle kinetics inside the stochastic layer. It is important for a description of the poloidal particle motion in the ergodic divertor of the tokamak. Recently a fractional type of kinetic equation was introduced in a set of publications [16] where a generalization of the ideas of Lévy flights [17,18] and fractal time [19] was described. Numerical analysis [20] and experimental data [21–23] provide a serious foundation for the fractional-type space-time kinetics. In Ref. [23] quantitative results were obtained for different distributions.

It is clear from the earlier publications [24,25,12] that transport properties of chaotic dynamics can be anomalous because of the presence of islands, the boundaries of islands are "sticky," and there are power laws in the distribution function, correlation functions, etc. Contemporary analysis of the anomalous transport becomes more sophisticated (see, for example, reviews [26,27]).

The aim of this article is twofold. The first is to analyze scaling properties for the separatrix map introduced in [2] (see also [3,11]). In Sec. II scaling properties of the particle dynamics inside the stochastic layer will also be studied. The existence of self-periodicity on the perturbation parameter rescaling will be shown. This property is studied analytically in Sec. III and numerically in Sec. IV. Scaling of the island chain will be revisited in Sec. V. The second aim is to present the simulations of the particle kinetics in a stochastic layer in Sec. VI and to show how its anomalous properties are dependent on the phase space pattern character in Secs. VI and VII. A bizarre feature of the kinetics is revealed in its self-similarity, which corresponds, as it is shown in this article, to the fractal time wandering process. There is a strong dependence of the level of self-similarity and intermittency on the parameters of the system. A specific case of the anomalous kinetics reduction to a regular (Gaussian) one is found in Sec. VIII.

II. THE BASIC MODEL AND SCALING PROPERTIES OF THE SEPARATRIX MAP

Consider the basic model of a particle motion in the two-wave potential with the Hamiltonian

$$H = p^2/2 - \omega_0^2 \cos x - \epsilon\omega_0^2 \cos(x - vt + \chi) \tag{2.1}$$

and the equation of motion

$$\ddot{x}+\omega_0^2 \sin x = -\epsilon\omega_0^2 \sin(x-\nu t+\chi) , \tag{2.2}$$

where ν is the perturbation frequency, ϵ is the dimensionless level of perturbation, ω_0 is the frequency of small amplitude oscillations, and χ is the constant phase of the perturbation.

The unperturbed motion is described by the Hamiltonian

$$H_0 = p^2/2 - \omega_0^2 \cos x . \tag{2.3}$$

There are elliptic points at $x = x_n = 2\pi n$, $p = 0$ (0 points) and hyperbolic points at $x = x_n = (2n+1)\pi$, $p = 0$ (X points) in the phase space (x,p). The separatrix of the unperturbed motion corresponds to the unperturbed energy $H_s = \omega_0^2$.

Below, the motion of the system (2.2) near the unperturbed separatrix map [2,3,11]

$$\begin{aligned} h_{n+1} &= h_n + \epsilon K_n \sin\phi_n , \\ \phi_{n+1} &= \phi_n + (\nu/\omega_0)\ln(32/|h_{n+1}|) , \end{aligned} \tag{2.4}$$

where $h_n = (H_n - \omega_0^2)/\omega_0^2$ is the dimensionless oscillation energy, $\phi_n = \nu t_n$ is the phase at the moment t_n when the particle is in the unperturbed separatrix vicinity, and n is the number of an iteration step. The parameter K_n is equal to

$$K_n = 4\pi(\nu/\omega_0)^2 \exp(\pi\sigma_n\nu/2\omega_0)/\sinh(\pi\nu/\omega_0) . \tag{2.5}$$

The value ϵK corresponds to Melnikov's integral [1] and K is its part that does not depend on ϵ. The parameter K_n depends on n through the $\sigma_n = \pm 1$ only: $\sigma_n = 1$ if $\dot{x}_n > 0$ and $\sigma_n = -1$ if $\dot{x}_n < 0$. This condition can be formulated using the variable

$$\sigma_{n+1} = \begin{cases} 1, & h_{n+1} > 0 \\ -1, & h_{n+1} < 0 \end{cases}$$

if $\sigma_n = 1$ and

$$\sigma_{n+1} = \begin{cases} 1, & h_{n+1} < 0 \\ -1, & h_{n+1} > 0 \end{cases}$$

if $\sigma_n = -1$.

The map (2.4) has been studied for more than two decades by numerous researchers. In particular, it is known that there is an ergodic layer for an arbitrarily small level of perturbation ϵ. The width of the ergodic layer depends on parameters ϵ and ν/ω_0. It was shown recently [4] that for $\nu/\omega_0 \gg 0$ the width of the ergodic layer can still be narrow even for the values of $\epsilon \gg 1$. Here the attention is focused on the dependence of the separatrix map on the perturbation parameter ϵ.

Let us consider the scale tranform of ϵ and h

$$\epsilon \to \lambda_\epsilon \epsilon, \quad h_n \to \lambda_\epsilon h_n \tag{2.6}$$

with a scaling parameter λ_ϵ. The map (2.4) transforms into

$$\begin{aligned} h_{n+1} &= h_n + \epsilon K \sin\phi_n , \\ \phi_{n+1} &= \phi_n + (\nu/\omega_0)\ln(32/|h_{n+1}|) - (\nu/\omega_0)\ln\lambda_\epsilon . \end{aligned} \tag{2.7}$$

Comparing the maps (2.6) and (2.7) one can see their identity in the cylinder phase space $(h, \phi \bmod 2\pi)$ if

$$(\nu/\omega_0)\ln\lambda_\epsilon = 2\pi m, \quad m = 0, \pm 1, \pm 2, \ldots \tag{2.8}$$

because ϕ is a phase variable. Equation (2.8) defines such values of the scaling parameter λ_ϵ, which preserve the separatrix map

$$\lambda_\epsilon(m) = \exp(2\pi m \omega_0/\nu) . \tag{2.9}$$

Using expressions (2.6) and (2.9), one can define the renormalization separatrix map transform (RSMT). Map (2.6) is invariant under the following renormalization transform:

$$\begin{aligned} &\hat{R}_\epsilon : \ \epsilon \to \epsilon\lambda_\epsilon(1), \quad h \to h\lambda_\epsilon(1) \\ &\lambda_\epsilon(1) = \exp(2\pi\omega_0/\nu) , \end{aligned} \tag{2.10}$$

where $\lambda_\epsilon(1)$ is defined from (2.9) for $m = 1$. It is important to mention that the renormalization group transform $\hat{R}_\epsilon$ includes a renormalization of energy scale by a factor $\lambda_\epsilon(1)$ in correspondence with (2.10). This implies the same kind of self-similarity for resonances of the separatrix map.

Let us say that the condition

$$\phi_{n+q} = \phi_n + 2\pi s \tag{2.11}$$

defines the resonance of order (q,s) if q and s are nonnegative integers. Then interacting of the second equation of (2.4) yields

$$\phi_{n+q} = \phi_n + \frac{\nu}{\omega_0} \sum_{j=1}^{q} \ln[32/|h_{n+j}(q,s)|] . \tag{2.12}$$

Let us consider a formal transformation

$$h = h'/\lambda \tag{2.13}$$

and substitute (2.13) into (2.12). It gives

$$\phi_{n+q} = \phi_n + \frac{\nu}{\omega_0} \sum_{j=1}^{q} \ln[32/|h'_{n+j}(q,s)|] + \frac{\nu}{\omega_0} q \ln\lambda . \tag{2.14}$$

After renormalization of the set of resonance values $h_n(q,s)$, the same q and a different s occur if

$$\lambda = \lambda(q,s') = \exp\left[2\pi \frac{\omega_0}{\nu}\frac{s'}{q}\right] \tag{2.15}$$

for any $s' = mq$ with integer m. The minimal value of m is $m = 1$, which gives

$$\lambda(q,q) = \exp(2\pi\omega_0/\nu) = \lambda_\epsilon . \tag{2.16}$$

In the case (2.15) the equation of motion (2.14) is reduced to

$$\phi_{n+q} - \phi_n = 2\pi(s - s') = 2\pi s'' , \tag{2.17}$$

which is a resonant condition for the renormalized energies (2.13).

III. RENORMALIZATION NEAR THE X POINT

The results of the preceding section are accurate for the separatrix map. Since the separatrix map is an approximation that works to some extent near the separatrix, it is useful to obtain scaling properties of a system in a straightforward way from the Hamiltonian of a system.

Consider a periodically perturbed Hamiltonian system

$$H(x,p,t)=H_0(x,p)+\epsilon H_1(x,t) , \tag{3.1}$$

where H_0 is the unperturbed Hamiltonian, ϵ is the dimensionless perturbation parameter ($\epsilon \ll 1$), and H_1 is periodic

$$H_1(x,t+T)=H_1(x,t) \tag{3.2}$$

with a period $T=2\pi/\nu$. Let the point $x=0$, $p=0$ be the X point of the unperturbed Hamiltonian H_0, thus the expansion

$$H_0(x,p)=\tfrac{1}{2}(p^2-\omega_0^2 x^2) \tag{3.3}$$

is valid near the point. With (3.1) and (3.3) we have near the X point up to a constant additive term

$$H(x,p,t)=\tfrac{1}{2}(p^2-\omega_0^2 x^2)+\epsilon H_1(x,t) . \tag{3.4}$$

The general idea of simplification of the dynamics near the separatrix and the X point is to approximate x in the perturbation term $H_1(x,t)$ by the unperturbed expression for x which comes from (3.3). This gives simply

$$\omega_0 t=\omega_0\int dx/\dot{x}=\int dx/(2h-x^2)^{1/2}$$
$$=\ln|x+(2h+x^2)^{1/2}|+\text{const} \tag{3.5}$$

with the dimensionless energy

$$h=(H_0-\omega_0^2)/\omega_0^2 . \tag{3.6}$$

It follows from (3.5) that the transform

$$h=\lambda h_\lambda, \quad x=\lambda^{1/2}x_\lambda, \quad \lambda>0 \tag{3.7}$$

leads to the time shift

$$\Delta t=\frac{1}{2\omega_0}\ln\lambda . \tag{3.8}$$

Let this shift be equal to the period T of the perturbation $H_1(x,t)$. Then

$$\lambda=\exp(2\omega_0 T)=\exp(4\pi\omega_0/\nu) . \tag{3.9}$$

Now let us add to (3.7) the transformation of momentum $p=\lambda^{1/2}p_\lambda$ and apply the full transform

$$\hat{R}_\lambda: \quad x=\lambda^{1/2}x_\lambda, \quad p=\lambda^{1/2}p_\lambda, \quad H=\lambda H_\lambda \tag{3.10}$$

to the initial Hamiltonian (3.1) in the vicinity of the X point, i.e., with H_0 in the form (3.3). The transformation (3.10) is canonical and gives the Hamiltonian (up to a constant)

$$H_\lambda=\tfrac{1}{2}(p_\lambda^2-\omega_0^2 x_\lambda^2)+\epsilon_\lambda H_1(\lambda^{1/2}x_\lambda,t) , \tag{3.11}$$

where

$$\epsilon=\lambda\epsilon_\lambda \tag{3.12}$$

and periodicity (3.2) has been used.

The obtained result can be formulated as follows: the scaling transformation (3.12) of the perturbation parameter preserves the form of the Hamiltonian of a system in the vicinity of the X point with the rescaling (3.7) of variables if one takes λ of an appropriate value (3.9) dependent on the period of the perturbation H_1. Therefore Eqs. (3.9)–(3.12) form the renormalization group near the X point. Comparing this result to the exact RSMT (2.9) and (2.10) one has

$$\lambda=\lambda_\epsilon^2(1) \tag{3.13}$$

or

$$\hat{R}_\lambda=\hat{R}_\epsilon^2 . \tag{3.14}$$

Equations (3.13) and (3.14) make a connection between renormalization properties of the separatrix map and the initial Hamiltonian. In particular, applying $\lambda_\epsilon(1)$ in (3.12) instead of λ we have

$$H_{\lambda_\epsilon}=\tfrac{1}{2}(p_{\lambda_\epsilon}^2-\omega_0^2 x_{\lambda_\epsilon}^2)+\epsilon_{\lambda_\epsilon}H_1(\lambda_\epsilon^{1/2}x_{\lambda_\epsilon},t+T/2) , \tag{3.15}$$

which means a time shift per half a period of the perturbation.

Taking into account the pictures obtained in the following section by simulation, one should note that the above renormalization transform (3.10)–(3.12) is valid for the phase portrait of a system only near the X point. Far from the X point the transform (3.10)–(3.12) changes the system's phase portrait topology. Numerical simulation of the existence of the renormalization group $\hat{R}_\lambda$ or $\hat{R}_\epsilon$ can be realized in a simple way. One should simply replace the parameter ϵ in the Hamiltonian by $\epsilon\lambda_\epsilon^m(1)$ and compare the obtained phase portraits. This will be demonstrated in the next section.

IV. SIMULATION OF THE RENORMALIZATION TRANSFORM

In order to obtain a good accuracy of computations and resolve a fine structure of the distribution function in the phase space, the symplectic integrator method was applied [28] with a simplification owing to the fact that the Hamiltonian (2.1) was separable. Special testing was done for three different realizations of the symplectic integrator: fourth order by Forest and Ruth [29] and fifth-order optimal by McLachlan and Pan [30]. The fifth-order optimal was selected with time step 0.02 and with a numerical data processor stack 0.005. With double precision a test orbit near the separatrix displayed the accuracy of computations of the order 10^{-14} for the computational time $t=1.5\times10^3$.

Figures 1(a) and 1(b) display phase portraits of the separatrix map (2.4) for positive velocity $\dot{x}>0$ and for two different values of ϵ such that $\epsilon_a=\lambda_\epsilon^2(1)\epsilon_b$ with $\lambda_\epsilon(1)=\exp(2\pi/5.4)=3.2013\ldots$. In spite of that, the difference between the values of ϵ is of one order (approximately), the two phase portraits in Fig. 1 are almost identical, and their slight deviation is due to $\lambda_\epsilon(1)$ being

taken with a finite number of digits of accuracy.

In Fig. 2 we present two Poincaré sections for the initial equation of motion (2.2) in the vicinity of the X point $(0,\pi)$. The values of ϵ and χ for the two cases in Figs. 2(a) and 2(b) are $\epsilon_a=0.01$, $\chi=0$ and $\epsilon_b=\lambda_\epsilon(1)\epsilon_a=0.032$, $\chi=\pi$. Two pictures in Fig. 2 are topologically similar because the difference in ϵ_a and ϵ_b corresponds to the renormalization scaling parameter $\lambda_\epsilon(1)$. At the same time there is a rescaling of sizes along the (x,p) axes. The difference between the portraits in Figs. 1 and 2 corresponds to different phase spaces: (h,ϕ) in Fig. 1 and (p,x) in Fig. 2. The important step in preparing Fig. 2 is a high resolution plot that creates a possibility to observe a similarity between Figs. 2(a) and 2(b) not only in the topological structure, but to indicate dark strips at similar locations as an indication of invisible cantori.

The renormalization property of the dynamics in a stochastic layer in the vicinity of the X point is a general property of systems of the type (3.1), whereas the scaling transformation parameter λ_ϵ can be of different forms. For example, consider two other Hamiltonians

$$H=p^2/2-a^2x^2/2+x^4/4-\epsilon\cos(x-\nu t+\chi)\ , \quad (4.1)$$

$$H=p^2/2-a^2x^2/2+x^4/4+\tfrac{1}{2}\epsilon x^4\sin(\nu t+\chi)\ . \quad (4.2)$$

In correspondence with the general consideration in Sec. III, we have to find the coefficient before the $-x^2/2$ term in the expansion near the X point. In (3.11) it is ω_0^2, which coincides with a square, small amplitude oscillation frequency. For the cases (4.1) and (4.2) this coefficient is a^2 and therefore the renormalization parameter is

$$\lambda_\epsilon(1)=\exp(2\pi a/\nu) \quad (4.3)$$

instead of (2.10).

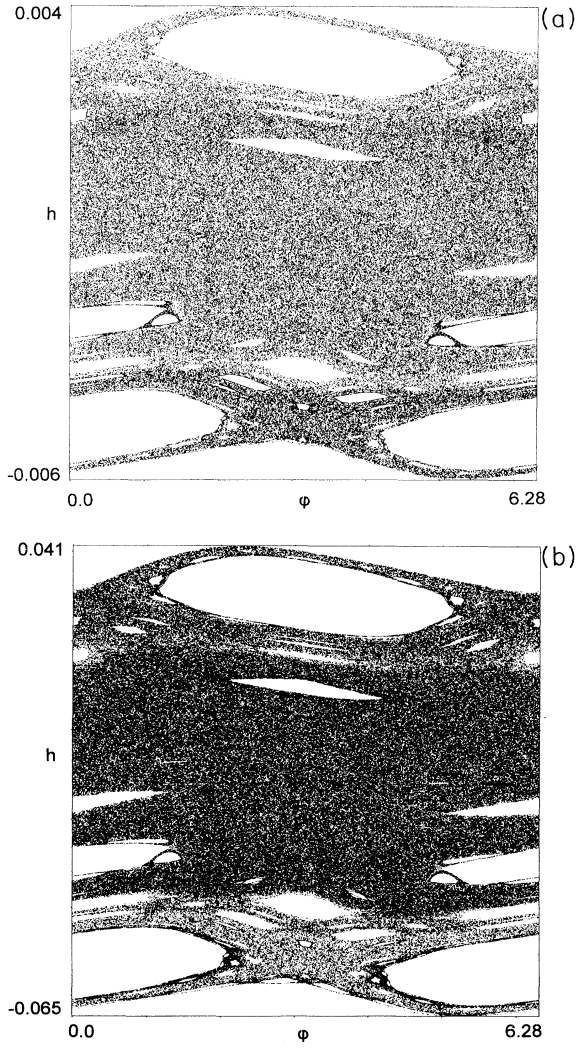

FIG. 1. Structure of an ergodic layer as described by the separatrix mapping (2.4) in the phase space $(\phi(\mathrm{mod}2\pi),h)$ with $\nu=5.4$, $\omega_0=1$, and for two values of ϵ: (a) $\epsilon=0.003\,124$ and (b) $\epsilon=0.032$. The number of iterations is 2×10^5 for each plot.

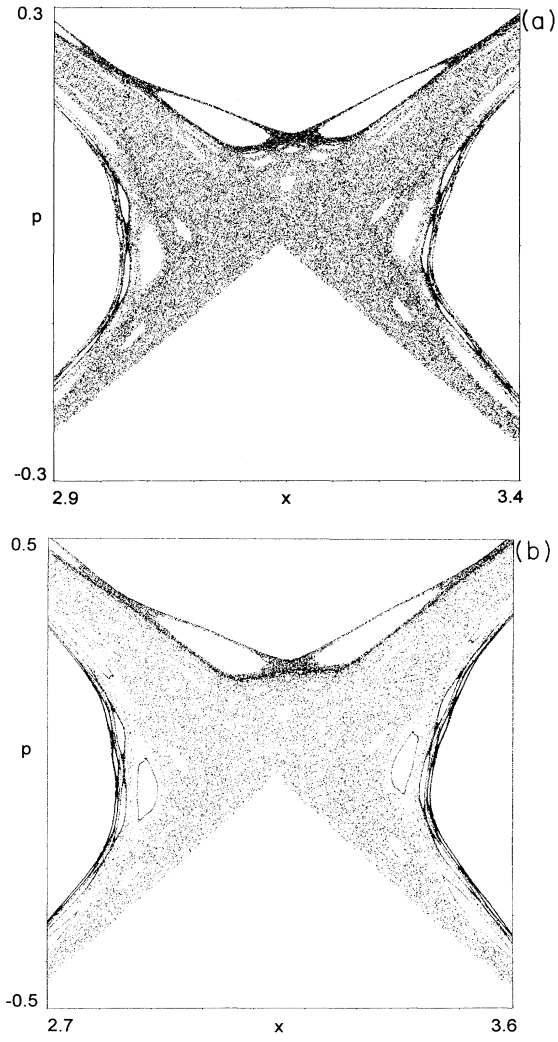

FIG. 2. Poincaré section of motion for Eq. (2.2) in the vicinity of the X point $(x=\pi, p=0)$ with the same ν,ω_0 as in Fig. 1. (a) $\epsilon_a=0.01$, $\chi=0$ and (b) $\epsilon_b=0.032$, $\chi=\pi$. The length of the orbits is 10^5 periods of perturbation for each of the four trajectories.

Our numerical simulation confirms the coincidence of the topological pattern near the X point (with the phase shift π) before and after the rescaling of the perturbation parameter

$$\epsilon \rightarrow \epsilon \exp(2\pi a/\nu) . \tag{4.4}$$

The values $a=1$, $\nu=5.4$, and $\epsilon=0.031$ are considered to correspond to $\lambda_\epsilon(1)=3.2013\ldots$.

In the next section the scaling properties of the islands in the phase portrait will be discussed.

V. SCALING OF SUBISLANDS

The topological structure of the stochastic layer is complicated and depends significantly on values of the perturbation parameter and the frequency. One such property—the persistence of the topology after rescaling ϵ—was demonstrated above. There are different sets of islands inside the stochastic layer, which are responsible for different properties of trajectories. Renormalization properties of chaotic dynamics inside the stochastic layer have been extensively studied in [4,31–33], especially in relation to the problem of islands-around-islands particles transport [31,12,34–36]. The plot in Fig. 3 demonstrates different roles of islands and their influence upon the particle transport.

The picture in Fig. 3(a) provides a full Poincaré section for six different orbits with a length of 3×10^5 periods of perturbation. Dark places correspond to regions of the orbit stickiness. The darker the region the longer the sticky event. Darkness in the middle part of the plot corresponds to "flights." Long, almost regular parts of the orbit are plotted in Fig. 3(b) where full (infinite in x) phase space (p,x) is considered, in contrast to Fig. 3(a), where the phase space is cylindrical $(p,x-\mathrm{mod}2\pi)$. The orbit in Fig. 3(b) corresponds to one of the orbits presented in Fig. 3(a) and the difference is only in the way the Poincaré section is plotted. The darkness around the main island on the bottom part in Fig. 3(a) corresponds to the orbit trapped in the area of a narrow boundary layer of the island. Competition between trappings and flights results in a transport law

$$\langle |x-\langle x\rangle| \rangle \sim t^{\mu} \tag{5.1}$$

with a transport exponent μ that can be different from the normal law case $\mu=\frac{1}{2}$.

In the past few years there were many studies of the influence of the islands-around-islands structure on the anomalous transport by a renormalization method [16,20] that introduces two different scaling parameters: λ_S, which corresponds to the area S scaling of islands of different generations, and λ_T, which corresponds to a characteristic time scaling for the same islands. It was proposed in [20] to use λ_T as the scaling parameter for periods of last invariant curves inside the islands set. Other time scales can be used also, but there exists a functional connection between different time sets and the λ_T corresponding to these sets.

To illustrate the existence of scaling we consider a set of subislands that belong to the main island on the bottom of Fig. 3(a). Variables related to the island values will be labeled 0. Variables for the next generations of the island will be labeled 1,2, ... Figure 4 presents close-ups of a few island generations. In analogy to [20] we prepare Table I with different values of the island-set properties.

Let ΔS_k be the area and T_k be the period of the last invariant curve inside an island of the kth generation. Table I shows the values of ΔS_k and T_k, the number of islands q_k in the chain of islands and different ratios. We introduce also the full area $\delta S_k=n_k\Delta S_k$ of islands in the kth generation chain. Table I makes evident the existence of scaling properties

$$\delta S_{k+1}=\lambda_S \delta S_k, \quad T_{k+1}=\lambda_T T_k \tag{5.2}$$

with scaling parameters

$$\lambda_S \sim 0.07, \quad \lambda_T \sim 8.9 \tag{5.3}$$

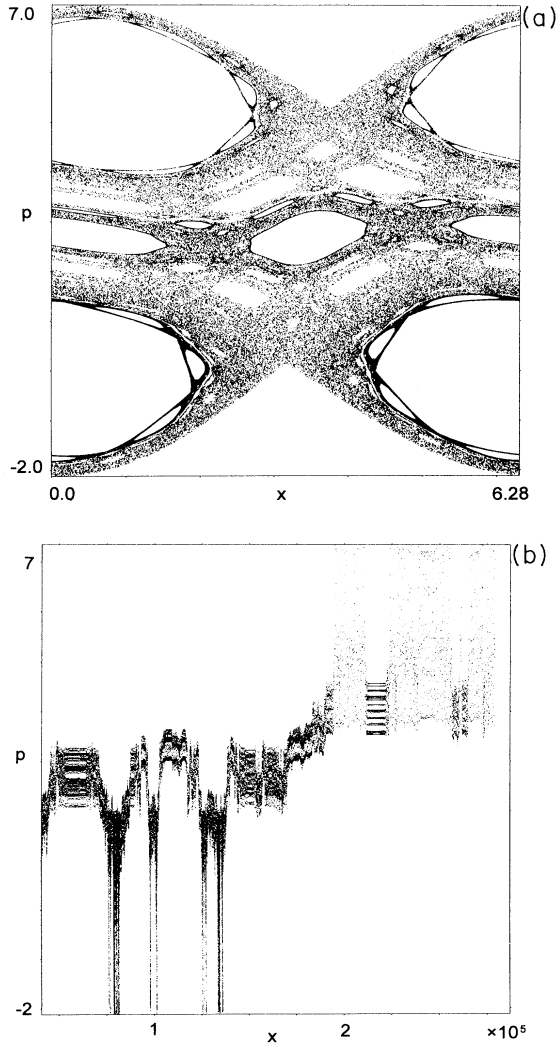

FIG. 3. Poincaré section of seven orbits indicates flights and trapping as dark regions (a) in cylindrical phase space and (b) in the infinite phase space. $\nu=5.4$, $\omega_0=1$, $\epsilon=0.9$, and $\chi=0$. The length of the orbits is 10^5 periods of perturbation.

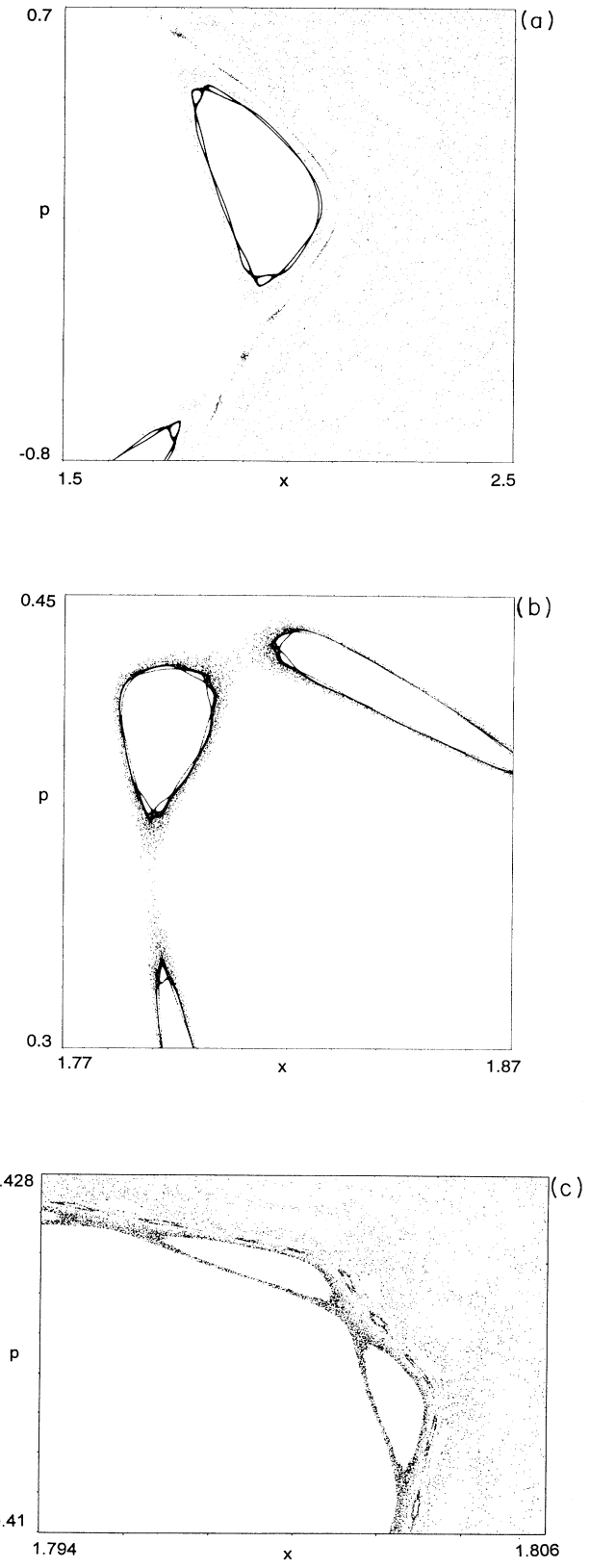

FIG. 4. Poincaré sections with islands of three generations (a), (b), and (c) for islands on the bottom of Fig. 3(a). The length of the orbits is 2.1×10^6 periods of perturbation.

approximately independent of k. One can observe small deviations from the constant values (5.3), which do not change the leading exponential dependence (5.2).

Some reasons for the observed dispersion of values of λ_S,λ_T can be mentioned: (i) we have considered only the first few generations, which is not enough to get a convergency; (ii) it could be a multifractal distribution of different values of λ_S,λ_T rather than a one-value fractal. The latter situation will be discussed further in the next section.

VI. DISTRIBUTION FUNCTION

There are two ways to consider particle transport in the stochastic layer: in cylindrical space (x mod2π) or in phase space infinite in x. Actually both of these presentations can be connected. Below the transport infinite in x is studied and we are interested in the probability function $P(x,t)$ to find a particle with position x at the time incident t inside the stochastic layer. There is also a normalization condition

$$\int P(x,t)dx = 1 \ . \tag{6.1}$$

For large time asymptotics the function $P(x,t)$ is well representative because the stochastic layer is narrow along the momentum p and one can neglect a transport process along p.

It is worth mentioning that the anomalous transport in the p direction for the standard map has been observed in a number of works [12,37–39] for the values of a perturbation parameter near a so-called threshold of transition to the global chaos or near the accelerated modes. In [12] there were also estimates for the power laws of the exit time distribution in the stochastic layer. Below, the anomalous transport features will be considered for the stochastic layer strictly (no transport along the p direction) with the main stress on fractal space-time properties inside the layer.

In addition to the evolution of the distribution function we consider its shifted moments as a function of time

$$R_m(t)\equiv\langle(x-\langle x\rangle)^m\rangle \quad (m>1) \ . \tag{6.2}$$

Expecting a power law dependence on x for $P(x,t)$, it is worth mentioning that the powerwise tail distribution functions are "inconvenient" to observe for the dynamical chaos. One should be ready to find different intermediate asymptotics for the exponents and strong fluctuations (see the detailed discussion in [36]). In addition to this difficulty, long flights and traps lead to a very slow convergence of the averaging procedure, which imposes a significant increase in the number of orbits over which an averaging is performed. Below we will illustrate these comments by presenting two different sets of data for two time scales.

The first set of data is related to the time length $t=10^4T$ and 3600 trajectories. The simulation was performed for $\nu=5.4$, $\omega_0=1$, and $\epsilon=0.9$. The Poincaré section for a few orbits is shown in Fig. 3(a). The distribution function $P(x,t)$ for $t=10^4T$, averaged over 3600 trajectories, is displayed in Fig. 5. Figure 5(a) features the

TABLE I. Self-similarity of three generations of islands.

k	q_k	T_k/T	T_{k+1}/T_k	ΔS_k	n_k	$\delta S_k = n_k \Delta S_k$	$\delta S_{k+1}/\delta S_k$
0	1	6.82		8.98	1	8.98	
1	7	6.1×10	8.94	9.45×10^{-2}	1×7	6.62×10^{-1}	0.074
2	9	5.4×10^{2}	8.85	6.55×10^{-4}	$1\times7\times9$	4.13×10^{-2}	0.062
3	9	4.8×10^{3}	8.89	5.44×10^{-6}	$1\times7\times9\times9$	3.08×10^{-3}	0.075

existence of a long tail, which corresponds to fast moving (ballistic) particles. A log-log plot of the tail is presented in Fig. 5(b). The graph shows a close to the linear dependence on $\log_{10}x$ with oscillations that increase at the end of the tail due to fewer events. It describes the initial stage of the distribution function evolution.

After a longer time the particles distribution becomes more symmetric, which is illustrated by the second set of data (Fig. 6) obtained after averaging over 7000 initial conditions with the length of the orbits 10^5T each. In spite of the long time of observation there are still large fluctuations because of particle trappings. The distribution function has a power-tail-like tail for the first set of data. If we suppose that for large x the asymptotics is valid

$$P(x,t)\sim 1/x^{\alpha+1}\ , \tag{6.3}$$

then $\alpha\sim(0.3\pm0.1)$ for the first set of data and the determination of α is not reliable for the second set of data in spite of the very large statistics (7000 orbits) and long computational time (10^5T). This does not permit us to say more about the real properties of the distribution function.

More informative results can be obtained from the moments (6.2) if we consider their large time asymptotics. In Fig. 7 the corresponding results are presented for the even values on $m=2n$ ($n=1-5$). The $\log_{10}R_{2n}$ vs $\log_{10}t$ plot displays two different time intervals with almost linear dependence, but with different exponents μ_m in the formula

$$R_m = R_{2n}(t)\sim t^{\mu_m}\quad (t\to\infty)\ . \tag{6.4}$$

It is clear from Fig. 7(a) that the crossover occurs at $t\sim4\times10^4$ T for two different regimes of the transport, as mentioned above. The linear dependence of $\log_{10}R_{2n}$ on $\log_{10}t$ is more evident for $t>4\times10^4T$ [see Fig. 7(b) for details]. Values of $\mu_m=\mu_{2n}$, obtained from Fig. 7(b), are plotted in Fig. 7(c) and obey the law

$$\mu_m=\mu_{2n}\simeq\mu_0+2\mu n \tag{6.5}$$

with $\mu_0=-0.02$ and $\mu=0.79$. We cannot find in a reliable way a nonlinear dependence of μ_{2n} on n as much larger computations are necessary to clarify the existence or nonexistence of the multiscale transport. A physical reason for the multifractal behavior could be the existence of several different resonance sets or several

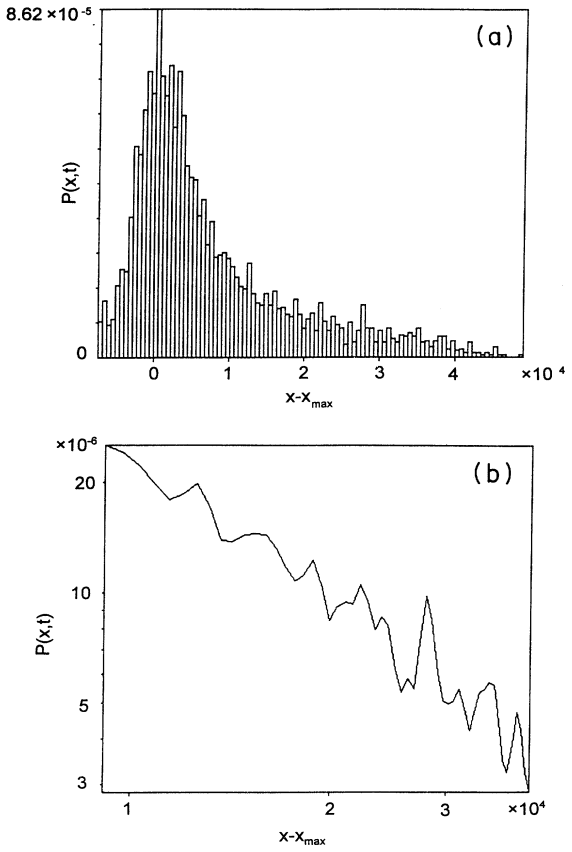

FIG. 5. Distribution function $P(x,t)$ versus x for $\nu=5.4$, $\omega_0=1$, $\epsilon=0.9$, $\chi=0$, and time incident $t=10^4T$. The data set is collected from 3600 trajectories. (a) The histogram of $P(x,t)$. (b) Log-log plot of the tail of $P(x,t)$.

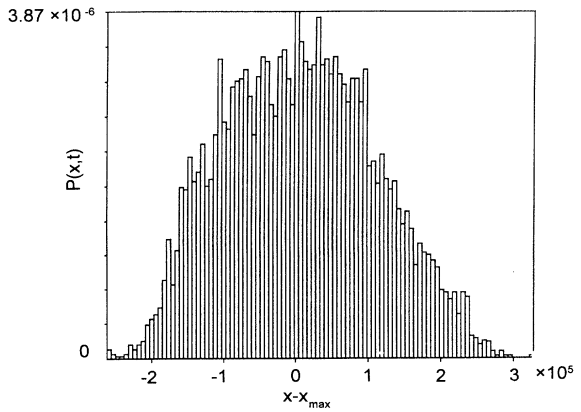

FIG. 6. Same as in Fig. 5(a), but for time incident $t_0=10^5T$. The statistics of the data set is collected from 7000 trajectories.

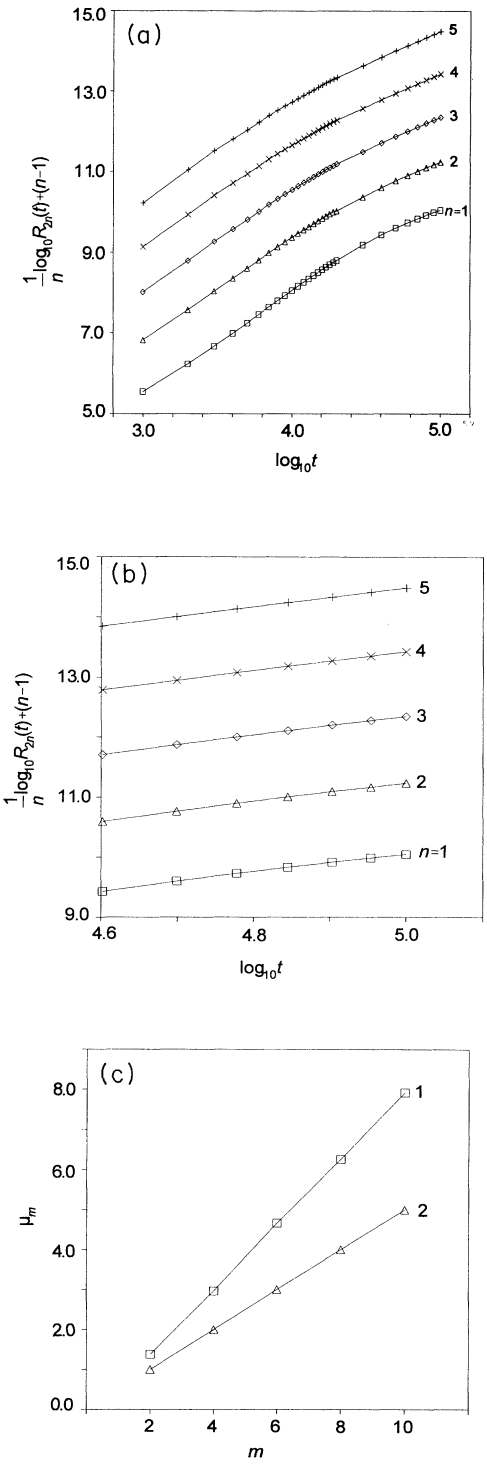

FIG. 7. Data for moments of the distribution function $P(x,t)$. (a) Plot of $(1/n)\log_{10}R_{2n}(t)+(n-1)$ vs $\log_{10}t$ for the time interval $10^3 \le t \le 10^5$. The shift $(n-1)$ is shown for convenience in displaying the curves. (b) Same as in (a) for the time interval $4\times10^4 \le t \le 10^5$ when the transient evolution is supposed to end. (c) Demonstration of the self-similarity: the straight line 1 corresponds to the values $\mu_m=\mu_{2n}$ from the data in (b) and line 2 corresponds to the Gaussian distribution and is given for comparison.

different island hierarchy systems. Each of them generates its own set of flights and its own set of scaling parameters λ_S and λ_T. It was shown in [16] that for some simplified situations

$$\mu=|\ln\lambda_S|/\ln\lambda_T \ . \tag{6.6}$$

One can find $\mu_2/2=0.61$ using the values (5.3), which does not contradict $\mu_2/2=0.69$ from Fig. 7(c).

VII. SELF-SIMILARITY NEAR THE X POINT AND PARTICLE TRANSPORT

Here we would like to pose a question rather than give an answer. Self-similarity due to the renormalization $\hat{R}_\lambda$ transform (3.9), (3.10), and (3.12)

$$\hat{R}_\lambda: \ H=\lambda H_\lambda, \quad \epsilon=\lambda\epsilon_\lambda, \quad \lambda=\exp(4\pi\omega_0/\nu) \tag{7.1}$$

has been described in Sec. III. Transform (7.1) preserves (mainly) a topology of the phase space near the X point. It is interesting to understand how this invariant property is resolved in the distribution function $P(x,t)$. The same question can be reformulated. The renormalization (7.1) preserves exactly the separatrix map form (see Sec. II). This means that the distribution function $P_S(x,t)$ for the stochastic layer of the separatrix map is invariant under the $\hat{R}_\lambda$:

$$\hat{R}_\lambda P_S(x,t)=\lambda_P P_S(\hat{x},\hat{t}) \ , \tag{7.2}$$

where λ_P is a constant that depends on λ and $\hat{x},\hat{t}$ are transformed variables x,t. We shall not extend this statement, but the existence of the invariant property of the distribution function $P_S(x,t)$ is evident. Now the reformulated question is, to what extent does the distribution function $P_S(x,t)$, generated by the separatrix map, represent the real transport properties of the system described by the original Hamiltonian (2.1)?

We hope that there exists a positive answer in a restricted form to this question. The main asymptotic properties of $P(x,t)$ and its moments $\langle x^m\rangle$ can be obtained from the separatrix map rather than by using the initial equation of motion (2.2). This conjecture seriously simplifies the problem of obtaining the transport exponent and related properties. Nevertheless, we cannot prove at the moment that the island set near the X point is a "leading" set responsible for the most "significant" flights and trappings. Plots of $P(x,t)$ versus x for 2000 trajectories during the time interval 2×10^4T for three different values of ϵ and χ: $\epsilon_a=\lambda_\epsilon^{-1}(1)\epsilon$, $\chi=\pi$; $\epsilon_b=\epsilon$, $\chi=0$; and $\epsilon_c=\lambda_\epsilon(1)\epsilon$, $\chi=\pi$ with $\nu=5.4$, $\omega_0=1$, $\epsilon=0.01$, and $\lambda_\epsilon(1)=\exp(2\pi/5.4)=3.2013\ldots$ (the same parameters as in Fig. 2) display the self-similarity of the three corresponding distributions. We plan to return to this issue in a future work.

VIII. A CASE OF NORMAL TRANSPORT

In this short section we would like to present an example of when, by an appropriate change in the two main parameters ϵ and ν/ω_0, one can significantly influence a character of transport. For the values $\epsilon=1$ and $\nu=2$

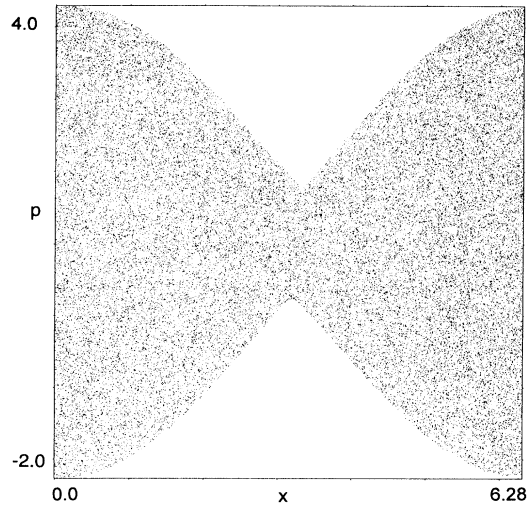

FIG. 8. Poincaré section for $\nu=2.05$, $\epsilon=1$, and $\chi=0$. The length of the orbit is 10^5 periods of perturbation.

($\omega_0=1$) there are no visible (or fairly large) islands. The corresponding Poincaré section is given in Fig. 8(a), where we introduce a small deviation of frequency $\nu=2.05$ ($\omega_0=1$) to show that an almost uniform and ergodic distribution exists in a finite domain around $\nu=2$. We have found that the corresponding distribution function is very close to the Gaussian one and that the transport is normal, i.e., diffusional, in the absence of the islands' structure [see curve 2 in Fig. 7(c)].

The described property of a possibility to control the transport is remarkable. For an application such as the poloidal transport in a tokamak with the ergodic divertor one can manipulate with the divertor field to reduce the possibility of the anomalous bunching of particles and to decrease the level of fluctuations of the loaded energy.

IX. CONCLUSIONS

The fine structure of the stochastic layer was always a problem of great interest and became more significant as the problem of anomalous transport in dynamical chaos arose for different applications. In this article we have considered a few related topics. We have derived an exact renormalization transform $\hat{R}_\epsilon$ for the separatrix map and shown that the transform $\hat{R}_\epsilon^2=\hat{R}_\lambda$ approximately preserves the dynamics near an unperturbed saddle (X) point. These results are confirmed by a high accuracy simulation. Exponential law for the local escape time near the saddle point was found in [40], which seems to be related to the self-similarity described above. Study of particle transport discovered the anomalous transport exponents and time intervals with different physical properties. It is shown that the anomalous behavior of the long term asymptotics for the moments of the distribution function can be tied to self-similar properties of the islands-around-islands construction. We have shown the persistence of the shape of the distribution function under the renormalization $\hat{R}_\epsilon$ transform. There exists a slight instability of the data depending on the existence of different intermediate asymptotics. It appears that the continuation of computations of $P(x,t)$ for longer times is desirable.

ACKNOWLEDGMENTS

We would like to express our gratitude to V. Rom-Kedar for useful comments. This work was supported by the U.S. Department of Energy, Grant No. DE-FG02-92ER54184, and by the U.S. Department of Navy, Grant No. N00014-93-1-0218.

[1] V. K. Melnikov, Dokl. Akad. Nauk **148**, 1257 (1963) [Sov. Math. Dokl. **4**, 266 (1963)].
[2] G. M. Zaslavsky and N. N. Filonenko, Zh. Eksp. Teor. Fiz. **54**, 1590 (1968) [Sov. Phys. JETP **25**, 851 (1968)].
[3] V. V. Chirikov, PHys. Rep. **52**, 263 (1979).
[4] D. Escande, Phys. Rep. **121**, 163 (1985).
[5] P. Holmes, J. Marsden, and J. Scheurle, Contemp. Math. **81**, 213 (1988).
[6] V. F. Lazutkin, I. G. Schachmanski, and M. B. Tabanov, Physica D **40**, 235 (1989); V. F. Lazutkin, Dokl. Akad. Nauk **313**, 268 (1990) [Sov. Math. Dokl. **42**, 5 (1991)]; V. G. Gelfreich, V. F. Lazutkin, and M. B. Tabanov, Chaos **1**, 137 (1991).
[7] C. Amick, S. C. E. Ching, L. P. Kadanoff, and V. Rom-Kedar, J. Nonlin. Sci. **2**, 9 (1993).
[8] V. V. Afanase'ev, A. A. Chernikov, R. Z. Sagdeev, and G. M. Zaslavsky, Phys. Lett. A **144**, 229 (1990).
[9] D. V. Treshchev (unpublished).
[10] G. M. Zaslavsky, Chaos **4**, 589 (1994).
[11] G. M. Zaslavsky, R. Z. Sagdeev, D. A. Usikov, and A. A. Chernikov, *Weak Chaos and Quasiregular Patterns* (Cambridge University Press, Cambridge, England, 1991).
[12] B. V. Chirikov and D. L. Shepelyansky, Physica D **13**, 394 (1984); B. V. Chirikov, Chaos, Solitons, Fractals **1**, 79 (1991).
[13] V. Rom-Kedar and S. Wiggins, Arch. Rat. Mech. Anal. **109**, 239 (1990); V. Rom-Kedar, Nonlinearity **7**, 441 (1994).
[14] V. Melnikov, in *Transport, Chaos, and Plasma Physics,* edited by S. Benkadda, F. Doveil, and Y. Elskens (World Scientific, Singapore, 1994), p. 126.
[15] A. Boozer *et al.*, New York University Report No. DOE/ER/53223-196, MF-125, 1992 (unpublished).
[16] G. M. Zaslavsky, in *Topological Aspects of the Dynamics of Fluids and Plasmas,* edited by H. Moffatt *et al.* (Kluwer, Boston, 1992), p. 481; Chaos **4**, 25 (1994); Physica D **76**, 110 (1994).
[17] P. Lévy, *Theories de l'Addition des Variables Aleatoires* (Gauthier-Villier, Paris, 1937).
[18] E. Montroll and M. Schlesinger, in *Studies in Statistical Mechanics,* edited by J. Lebowitz and E. Montroll (North-Holland, Amsterdam, 1984), Vol. 11, p. 1.
[19] M. F. Shlesinger, Annu. Rev. Phys. Chem. **39**, 269 (1988); Physica D **38**, 304 (1989); H. Scher, M. F. Shlesinger, and

J. T. Bendler, Phys. Today **44** (1), 26 (1991).
[20] G. M. Zaslavsky, D. Stevens, and H. Weitzner, Phys. Rev. E **48**, 1683 (1993).
[21] O. Cardoso and P. Tabeling, Europhys. Lett. **7**, 225 (1988); Eur. Mech. J. B **8**, 459 (1989).
[22] R. Ramshankar, D. Berlin, and J. P. Gollub, Phys. Fluids A **2**, 195 (1990); R. Ramshankar and J. P. Gollub, *ibid.* **3**, 1344 (1991).
[23] T. H. Solomon, E. R. Weeks, and H. L. Swinney, Phys. Rev. Lett. **71**, 3975 (1993).
[24] C. F. F. Karney, Phyisca D **8**, 360 (1983).
[25] V. V. Beloshapkin and G. M. Zaslavsky, Phys. Lett. **97A**, 121 (1983).
[26] J.-P. Bouchaud and A. Georges, Phys. Rep. **195**, 127 (1990).
[27] M. F. Shlesinger, G. M. Zaslavsky, and J. Klafter, Nature **363**, 31 (1993).
[28] Feng Kang and Qin Meng-Zhao, in *Numerical Methods for PDE,* edited by Zhu You-lan and Guo Ben-yu, Lecture Notes in Mathematics Vol. 1297 (Springer, New York, 1987), p. 1.
[29] E. Forest and R. Ruth, Physica D **43**, 105 (1990).
[30] R. McLachlan and P. Atela, Nonlinearity **5**, 541 (1992).
[31] R. S. Mackay, J. D. Meiss, and I. C. Percival, Physica D **27**, 1 (1987).
[32] J. D. Meiss and E. Ott, Physica D **20**, 387 (1986).
[33] J. D. Meiss, Rev. Mod. Phys. **64**, 795 (1992).
[34] T. Geisel, A. Zacherl, and G. Radons, Phys. Rev. Lett. **59**, 2503 (1987); Z. Phys. B **71**, 117 (1988).
[35] T. Geisel, J. Wagenhuber, P. Niebauer, and G. Obermain, Phys. Rev. Lett. **64**, 1581 (1990).
[36] V. V. Afanasiev, R. Z. Sagdeev, and G. M. Zaslavsky, Chaos **1**, 143 (1991).
[37] R. Ishizaki, H. Hata, T. Horita, and H. Mori, Prog. Theor. Phys. **84**, 179 (1990); R. Ishizaki, T. Horita, T. Kobayashi, and H. Mori, *ibid.* **85**, 1013 (1991).
[38] J. Klafter, G. Zumofen, and M. F. Shlesinger (unpublished).
[39] S. Benkadda, Y. Elskens, and B. Ragot, Phys. Rev. Lett. **72**, 2859 (1994).
[40] V. Rom-Kedar, in *Transport, Chaos, and Plasma Physics* (Ref. [14]), p. 39; Nonlinearity **7**, 441 (1994).